Observations of offshore low-level jets off the U.S. East Coast reveal systematic biases in ERA5 and HRRR

N. Bodini[1], S. Letizia[1], B. Adler[2,3], D.D. Turner[4], R. Krishnamurthy[5], A. Scholbrock[1], D. Jager[1], E. Cinquino[6], A. Kirincich[6]

[1]National Laboratory of the Rockies, Golden, CO, USA
[2]Cooperative Institute for Research in Environmental Sciences, Boulder, CO, USA
[3]Physical Sciences Laboratory, National Oceanic and Atmospheric Administration, Boulder, CO, USA
[4]Global Systems Laboratory, National Oceanic and Atmospheric Administration, Boulder, CO, USA
[5]Pacific Northwest National Laboratory, Richland, WA, USA
[6]Woods Hole Oceanographic Institution, Woods Hole, MA, USA

Key Points:

- WFIP3 offshore barge observations show frequent low-level jets during summer off the U.S. East Coast.
- HRRR and ERA5 underestimate low-level jet wind speed.
- Temperature profiles in models poorly represent the observed thermal structure.

Corresponding author: Nicola Bodini, `nicola.bodini@nlr.gov`

Abstract

Low-level jets (LLJs)—wind speed maxima typically occurring a few hundred meters above the surface—are common off the U.S. East Coast and influence many atmospheric processes with societal importance, including cloud formation, aviation safety, and search-and-rescue. However, their vertical structure and frequency remain poorly quantified due to limited offshore observations. This study presents new scanning Doppler lidar and infrared spectroradiometer data from the 2024 summer deployment of an offshore barge during the Wind Forecast Improvement Project 3. These coupled wind and temperature profiles provide unprecedented resolution to assess LLJ behavior and model performance. LLJs occurred in over 21% of observed profiles, with a weak diurnal preference for nighttime and early morning hours and maximum winds typically near 300 m. Both ERA5 and HRRR analysis underestimate jet wind speeds and misrepresent the boundary layer thermal structure. These results highlight persistent model biases and the critical need for high-resolution offshore observations.

Plain Language Summary

Understanding how wind behaves just above the ocean surface is essential for many applications: weather prediction, aviation safety, and search-and-rescue. One key feature in this environment is the low-level jet (LLJ)—a layer of fast-moving air a few hundred meters above the sea. LLJs can change how much power wind turbines produce and affect how weather models predict wind conditions. However, scientists so far have had limited opportunities to observe LLJs in detail over the ocean, especially far from land. In this study, we used advanced instruments placed on a barge off the coast of Massachusetts and Rhode Island to measure wind and temperature profiles up to a few kilometers above the ocean surface throughout summer 2024. We found that LLJs occurred over 21% of the time and peaked around 300 meters high. We then compared these measurements with widely used weather models and discovered that both models underestimated the strength of LLJs and did not capture the layering of temperature as well as the observations did. These results show why high-quality offshore measurements are so important: they help improve models that guide weather forecasting over the ocean.

1 Introduction

Offshore wind resource assessment and weather forecasting critically depend on advancing our understanding of the marine atmospheric boundary layer (MABL), which is governed by complex, multiscale processes that remain insufficiently observed and poorly represented in numerical models (Shaw et al., 2022). The MABL over coastal and open-ocean environments exhibits complex and seasonally varying thermodynamic stability (Archer et al., 2016), strong surface-atmosphere coupling (Patton et al., 2019), and frequent occurrences of low-level jets (LLJs) (Aird et al., 2022), each of which contributes to sharp vertical wind shear, directional veer, and enhanced wind turbine wake persistence (Lundquist et al., 2019; Platis et al., 2018). These phenomena remain key sources of uncertainty in both mesoscale and microscale modeling frameworks (Veers et al., 2019). The scarcity of high-resolution observations offshore that span the whole MABL—particularly with colocated wind and temperature profiles—limits model validation and development (Gottschall et al., 2014; Shaw et al., 2020; Viselli et al., 2019), and addressing these gaps is essential for reducing uncertainty in wind resource characterization (Barthelmie et al., 2021; Christiansen & Hasager, 2005).

Among the processes that challenge accurate offshore wind characterization and forecasting, LLJs are especially influential due to their impact on wind profile variability (Banta et al., 2006), cloud formation (Bosart & Sanders, 1981; Su et al., 2016), wind turbine loading and wake interactions (Gutierrez et al., 2017; Storm et al., 2008), and aviation safety (Liu et al., 2014). LLJs are characterized by a localized maximum in wind speed at low altitudes, typically a few hundred meters above the surface. They can occur under a range of synoptic and mesoscale conditions (Baas et al., 2009; Rife et al., 2010). In offshore regions, LLJ formation is commonly linked to baroclinic effects from land–sea temperature contrasts and synoptic-scale pressure gradients, with inertial oscillations playing a secondary modulating role (Angevine et al., 2006; Blackadar, 1957; de Jong et al., 2023; Holton, 1967). Unlike the classical continental Blackadar mechanism, offshore sites experience little diurnal variation in sea surface temperature, so inertial oscillations alone are not expected to dominate. Instead, stable stratification develops when warm continental air is advected over the relatively cool ocean surface. As noted by Shaw et al. (2022), the presence of a large continental landmass immediately upwind under prevailing westerly and southwesterly flow subjects the U.S. East Coast to strong continental boundary layer advection. This creates distinct baroclinic forcing and thermodynamic stability regimes compared to regions like the North Sea, where the prevailing fetch and geography differ. This land–sea thermal contrast, particularly active during the summer (Bodini et al., 2019), drives LLJ formation. The resulting diurnal modulation of LLJ occurrence is therefore weaker than in the classical continental case, with synoptic and baroclinic forcing playing a comparatively larger role.

Despite their importance, the vertical structure and temporal evolution of offshore LLJs remain poorly quantified in U.S. waters. This is primarily due to a persistent lack of observations that span the entire MABL. Most available measurements have come from buoy-mounted profiling lidars, which typically do not extend above 200 m and often fail to capture the jet nose (Aird et al., 2022; Debnath et al., 2021). A few ship-based or scanning lidar campaigns have provided deeper snapshots of LLJs, revealing noses as high as 600 m (Mahrt et al., 2014; Pichugina et al., 2017), but these are limited in duration and spatial coverage.

In the absence of widespread high-resolution observations, most assessments of offshore wind conditions rely on numerical weather prediction models or reanalysis products. However, extensive evaluation of the performance of these tools offshore has largely been confined to European waters, such as the North and Baltic Seas (e.g., Floors et al., 2013; Hallgren et al., 2020; Kalverla et al., 2020; Rubio et al., 2022; Schulz-Stellenfleth et al., 2022; Wagner et al., 2019). In contrast, model performance over U.S. offshore regions has undergone only limited validation (e.g., Myers et al., 2024; Pronk et al., 2022). As a result, significant uncertainty persists in both long-term energy yield estimates and short-term operational forecasts, particularly in U.S. environments dominated by LLJs.

To address this need, we leverage unique temperature and wind profiling observations from the third Wind Forecast Improvement Project (WFIP3). These data, collected using a scanning Doppler lidar and an infrared spectroradiometer deployed on a stationary barge in an active offshore wind lease area near Massachusetts and Rhode Island, provide unprecedented vertical and temporal coverage of the MABL—reaching altitudes up to a few kilometers across multiple months. These measurements represent the first coupled offshore observations of wind and thermal structure in this region with wind profile vertical resolution of 20–30 m, and temperature profile retrieval grid spacing of 10–50 m in the lowest 500 m, sufficient to resolve the nose and vertical shear of LLJs and evaluate their representation in models. In this study, we use these observations to systematically assess LLJ frequency, structure, and diurnal evolution over the summer months, when LLJs are the most frequent in this region. We then compare the observed profiles to wind and temperature fields from commonly used numerical datasets, quantifying model biases in jet frequency, nose height, peak speed, and temperature. We describe the WFIP3 field campaign, the observed and modeled data used in this study, and the LLJ detection process in Section 2. Section 3 compares observed and modeled wind speed and temperature profiles, and we conclude and suggest future work in Section 4.

2 Data and Methods

2.1 WFIP3 and its Offshore Barge

WFIP3 is a multi-institutional field campaign designed to advance the understanding and forecasting of the evolution of the MABL. Primarily funded by the U.S. Department of Energy and the National Oceanic and Atmospheric Administration (NOAA), WFIP3 is focused on the southern New England offshore region. The campaign includes both coastal and offshore deployments of advanced atmospheric and oceanographic instrumentation, operating from late 2023 through summer 2025. A central asset of the campaign was a heavily instrumented barge deployed ∼50 km south of Martha's Vineyard between June and September 2024 (Fig. 1). The barge hosted an array of scanning and profiling Doppler lidars, a ceilometer, an infrared spectroradiometer, and other in situ and remote sensing meteorological instruments, enabling observed profiles of wind with 20–30 m vertical resolution, and temperature and humidity with retrieval grid spacing of 10–50 m in the lowest 500 m.

2.2 Observations

The atmospheric observations used in this analysis were collected from one profiling and one scanning Doppler lidar and an infrared spectroradiometer deployed on the WFIP3 barge. A Halo Photonics Streamline XR+ scanning Doppler lidar (Pearson et al., 2009) was mounted atop a shipping container on the barge (Fig. 1) and operated in vertical profiling mode using a fixed 60° elevation angle. The system provided line-of-sight wind velocities with a range gate resolution of 30 m. Due to the instrument's blind zone, usable data began approximately 100 m above the instrument. At lower heights, wind speed was measured with a Windcube v2.1 profiling lidar using a Doppler-beam-swinging technique. The system provides a vertical profile every 4 s, beginning at 40 m above the instrument and extending upward in 20 m increments. For both lidars, only measurements with a carrier-to-noise ratio higher than −23 dB and a lidar-reported data availability exceeding 80% were retained. Wind profiles were derived from the line-of-sight velocities using a velocity-azimuth display algorithm with chi-square minimization. All lidar measurements were corrected for barge motion using high-frequency inclinometer data recorded on board, following the methodology described in Krishnamurthy et al. (2023) and Newsom et al. (2024). The wind speed uncertainty after motion correction, averaged over 10-minute intervals, is estimated to be less than 0.25 m s^{-1} in the lowest 1 km (Newsom et al., 2017), which is negligible compared to the model biases reported in Section 3.

In addition, an ASSIST-II infrared spectroradiometer measured downwelling infrared spectral radiance with a sampling rate of 14 s (Michaud-Belleau et al., 2025). From its observations, we retrieved quasi-instantaneous vertical profiles of temperature and humidity every 10 minutes using the Tropospheric Remotely Observed Profiling via Optimal Estimation (TROPoe) algorithm (Turner & Löhnert, 2014; Turner & Blumberg, 2019; Turner & Löhnert, 2021). TROPoe also assimilated cloud base height, surface temperature, pressure, and relative humidity from colocated instruments (Newsom et al., 2019). The TROPoe algorithm retrieves temperature and humidity profiles on a vertical grid spaced at 10-20 m near the surface, coarsening to 50 m across the LLJ nose region (100–500 m), and 160 m at 1.5 km. However, the effective vertical resolution of the retrieved profiles is coarser, with a resolution of 10 m near the surface, broadening to 100 m at 200 m altitude, and 1 km at 1.5 km (Letizia et al., 2025). This coarse resolution still provides approximately 2 independent pieces of information on the temperature profile across the rotor layer.

The timeline of available observations is shown in Fig. 1. This study only includes data collected when the barge was stationary at its final offshore deployment location, which totaled 87 days. To compare the lidar and ASSIST observations with the hourly

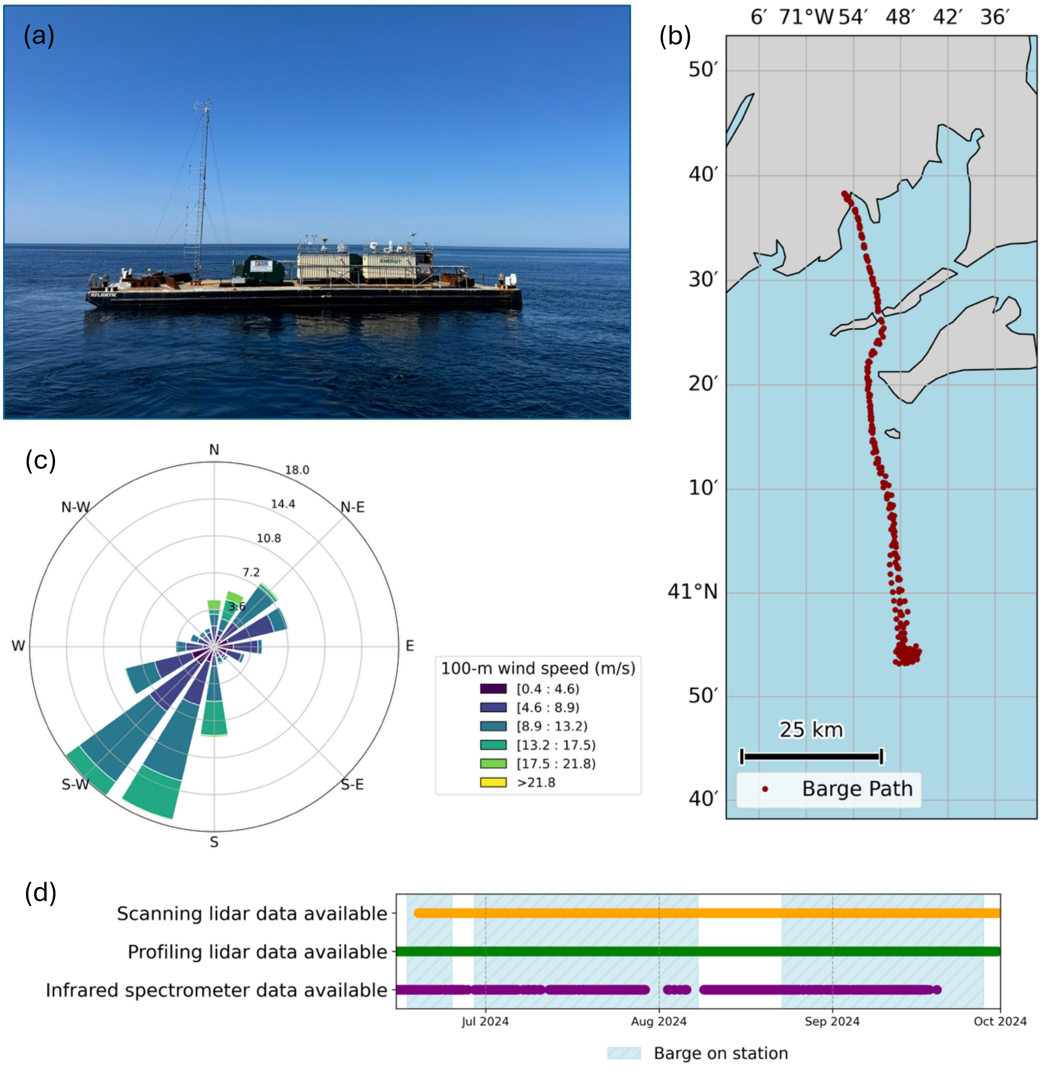

Figure 1. (a) Picture of the WFIP3 barge (credit Eve Cinquino, WHOI). (b) Map showing the barge deployment path and its final deployment location south of Martha's Vineyard. (c) 100-m wind rose from the barge profiling lidar. (d) Timeline of the barge instruments used in this analysis.

instantaneous model outputs, we select the wind and temperature profiles (10-minute averages for the lidars, quasi-instantaneous for the ASSIST) that are closest in time to each model timestamp. We also only include model data at the time stamps where corresponding observations are available.

2.3 ERA5 Data

To evaluate reanalysis wind and temperature profiles, we used ERA5 (Hersbach et al., 2020) model-level data at the grid cell closest to the deployment location of the WFIP3 offshore barge. Specifically, we retrieved u and v wind components, temperature, surface pressure, and specific humidity at 1-hour resolution from model levels spanning the lowest $\sim$2 km of the atmosphere. Heights were computed via hydrostatic integration using the ERA5 hybrid A and B coefficients and virtual temperature. The height resolution is approximately 20 m near the surface, increasing to $\sim$140 m at 1.5 km.

2.4 HRRR Data

In addition to ERA5, this analysis includes data from the High-Resolution Rapid Refresh (HRRR) model, a NOAA-developed and operated convection-allowing numerical weather prediction system specifically designed to provide detailed short-term forecasts over the contiguous United States. HRRR is run at a horizontal resolution of 3 km with 50 vertical layers (nine layers are within the lowest 1 km). The model is restarted hourly, using advanced data assimilation of radar, satellite, radiosonde, aircraft, and surface observations to derive initial conditions for the modeling system (Dowell et al., 2022; James et al., 2022). The physics within the HRRR is under continuous improvement (see Dowell et al., 2022, for details), incorporating the lessons learned from other WFIP field campaigns (e.g., Olson et al., 2019). For this study, HRRR model output was used to extract profiles of wind speed and temperature at the location of the WFIP3 offshore barge from the operational analysis fields (i.e., at forecast hour 0). The column data are interpolated from native model levels to fixed height levels, more closely spaced near the surface (e.g., every 10–20 m below 200 m), and increasing to coarser intervals aloft (100 m at 1.5 km).

2.5 Low-Level Jet Detection

To identify LLJs in both observations and modeled data, we applied an automated detection algorithm adapted from Vanderwende et al. (2015) and Quint et al. (2025) to each vertical profile of wind speed sampled at hourly resolution. An LLJ was flagged when the profile exhibited (i) a distinct wind speed maximum below 800 m (the "nose"), (ii) a minimum decrease of 3 m s^{-1} in wind speed above the nose within 400 m, and (iii) a peak wind speed of at least 10 m s^{-1}. Observed profiles lacking sufficient vertical resolution or coverage (fewer than 10 valid levels below 1200 m) were excluded from the analysis. For profiles meeting these criteria, we extracted the nose height and categorized the LLJs into four strength-based classes (0–3) based on combinations of nose wind speed (ws) and shear above the nose:

- Class 0: $10\,\mathrm{m\,s^{-1}} \le \mathrm{ws_{nose}} < 12\,\mathrm{m\,s^{-1}}$ and shear above nose $< 5\,\mathrm{m\,s^{-1}}$
- Class 1: $\mathrm{ws_{nose}} \ge 12\,\mathrm{m\,s^{-1}}$ and shear $\ge 5\,\mathrm{m\,s^{-1}}$
- Class 2: $\mathrm{ws_{nose}} \ge 16\,\mathrm{m\,s^{-1}}$ and shear $\ge 8\,\mathrm{m\,s^{-1}}$
- Class 3: $\mathrm{ws_{nose}} \ge 20\,\mathrm{m\,s^{-1}}$ and shear $\ge 10\,\mathrm{m\,s^{-1}}$.

This approach combines a falloff threshold with shear-based strength classification (Vanderwende et al., 2015; Quint et al., 2025), motivated by the argument of Hallgren et al. (2023) that rotor-layer shear—rather than the mere existence of a speed maximum—governs turbine loading and power production. The minimum nose speed of 10 m s^{-1} restricts detection to jets with direct relevance to wind turbine inflow. As demonstrated by Hallgren et al. (2023), LLJ frequency and morphology are sensitive to both the detection definition and vertical data window; cross-study comparisons should therefore be made with caution.

3 Results

LLJs were a recurring feature during the summer 2024 deployment of the WFIP3 barge. Time-height cross sections of mean wind speed from lidar observations and model outputs (Fig. 2a) show frequent nocturnal LLJs, most pronounced between 00 UTC and 10 UTC. These structures are also visible in the time-averaged wind profiles (Fig. 2c), with a characteristic wind speed maximum between 200 and 400 m. Both ERA5 and HRRR capture the mean LLJ structure but systematically underestimate wind speed by approximately -1 m s^{-1}, while well capturing the mean nose height near 300 m. The numerical datasets have a marginally better performance in representing the observed temperature (Fig. 2b and d): both ERA5 and HRRR have a slight positive bias compared to the temperature data retrieved from the infrared spectroradiometer observations. Near the surface, HRRR generally depicts a temperature inversion, which is not seen in the mean observations.

Applying the LLJ detection algorithm to the barge hourly lidar dataset reveals that more than 21% of the over 1900 quality-controlled profiles contained an LLJ. On the other hand, only about 14% of the HRRR profiles and 13% of the ERA5 profiles were classified as LLJs. Figure 3 summarizes four key LLJ characteristics—nose height, time of occurrence, LLJ class, and nose wind direction—for observations and model outputs. Observed LLJ noses span the lowest 800 m (the algorithm's vertical upper threshold), with a peak in frequency between 200 and 300 m, whereas HRRR and ERA5 both locate most LLJ occurrences between 100 and 500 m. ERA5 also misses most occurrences below 200 m. LLJs were observed at all times, with a peak in the local night and slightly lower frequency during the day. We note that the number of valid observed profiles remained relatively constant throughout the day, suggesting that the weak diurnal cycle in LLJ frequency is unlikely to be an artifact of data availability. The diurnal cycle of LLJ occurrence is relatively well represented by both numerical models, though ERA5 underrepresents LLJ frequency during the morning hours (12–17 UTC). Most detected LLJs were classified as Class 0 (weakest) or Class 1. HRRR tracked the observed distribution quite well while most of the LLJs detected in the ERA5 data were in class 0. Finally, most LLJ events were observed for winds from the southwest (dominant wind directions in the summer, Fig. 1), with a secondary peak observed for easterly-northeasterly winds. While a secondary peak is also simulated by both HRRR and ERA5, both models overestimate its frequency. A wind-direction-stratified analysis of the diurnal cycle was not feasible given the dominance of southwesterly flow during the deployment (Fig. 1), and remains an important target for future studies.

Model biases in wind speed exhibit diurnal and vertical patterns (Fig. 4a). Across all hours, both models show modest negative biases (generally around or less than 1 m s^{-1}), with HRRR showing fewer periods with statistically significant differences compared to ERA5. These biases substantially exceed the precision uncertainty of the Doppler lidar systems (typically below 0.1–0.2 m s^{-1}). However, during periods with LLJs (Fig. 4b), wind speed biases intensify: both models underestimate winds by up to 3 m s^{-1}—particularly within the lowest 1 km, where the noses of LLJs reside. Interestingly, the largest bias in ERA5 occurs at around 15 UTC (11 a.m. local time), where the frequency of detected LLJs in ERA5 is at its minimum. Temperature biases are presented in Fig. 4c. On average, both models exhibit warm biases throughout the vertical profile, with HRRR showing particularly pronounced overestimation at higher altitudes, and some negative bias close to the surface in the second half of the UTC day. During LLJ periods (Fig. 4d), both models display a characteristic pattern of warm biases near the surface, cold biases

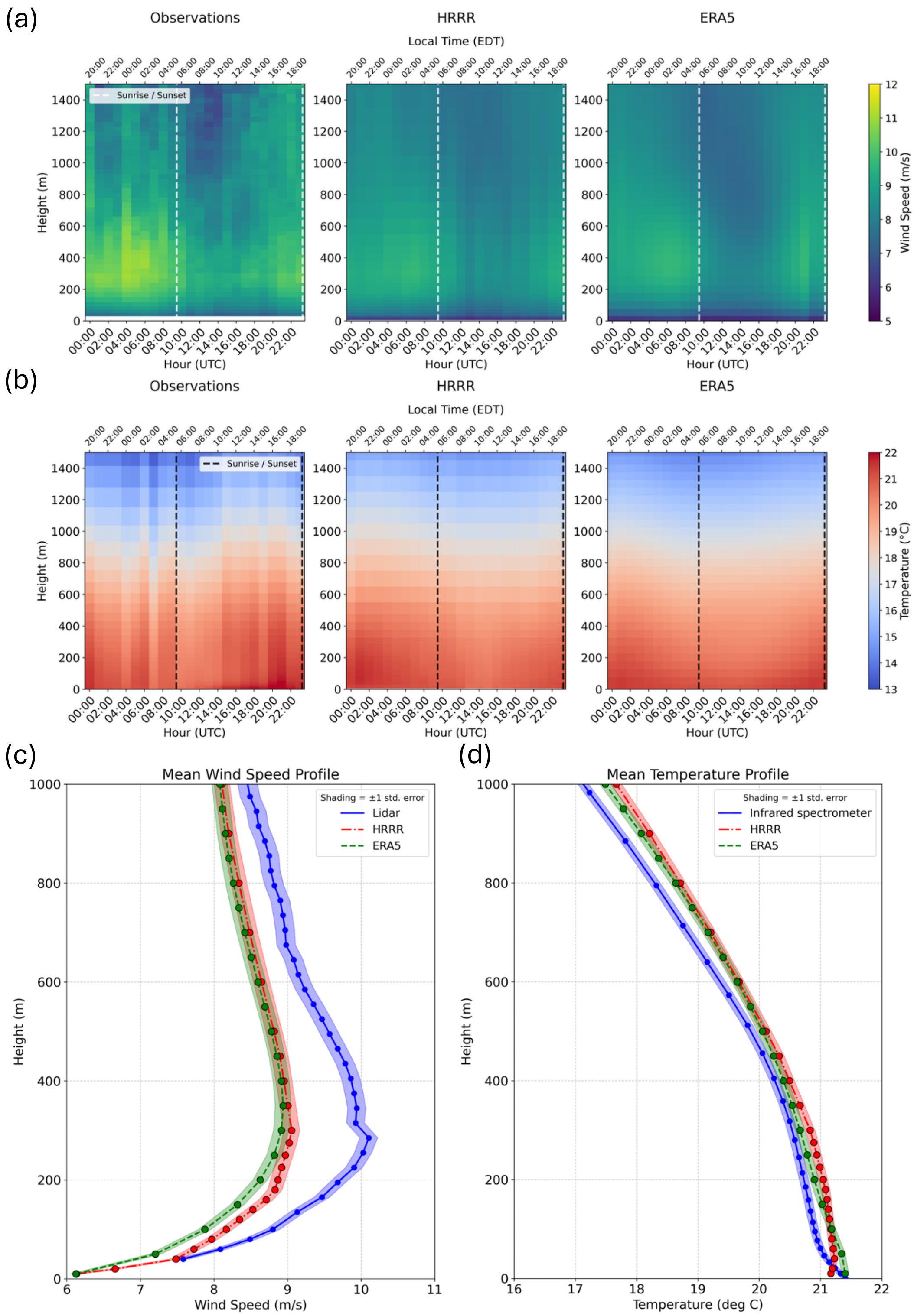

Figure 2. (a) Mean time-height cross sections of wind speed as observed by the barge lidars (left) and modeled by HRRR (center) and ERA5 (right). (b) Mean time-height cross sections of temperature as observed by the barge infrared spectroradiometer (left) and modeled by HRRR (center) and ERA5 (right). (c) Mean wind speed profiles from the barge lidar, HRRR, and ERA5, each plotted on their respective native vertical grids. Dots indicate the height levels at which data are available. Shading represents ±1 standard error of the mean. All datasets are restricted to the same valid time window. (d) As in (c) but for temperature, with observations from the barge infrared spectroradiometer.

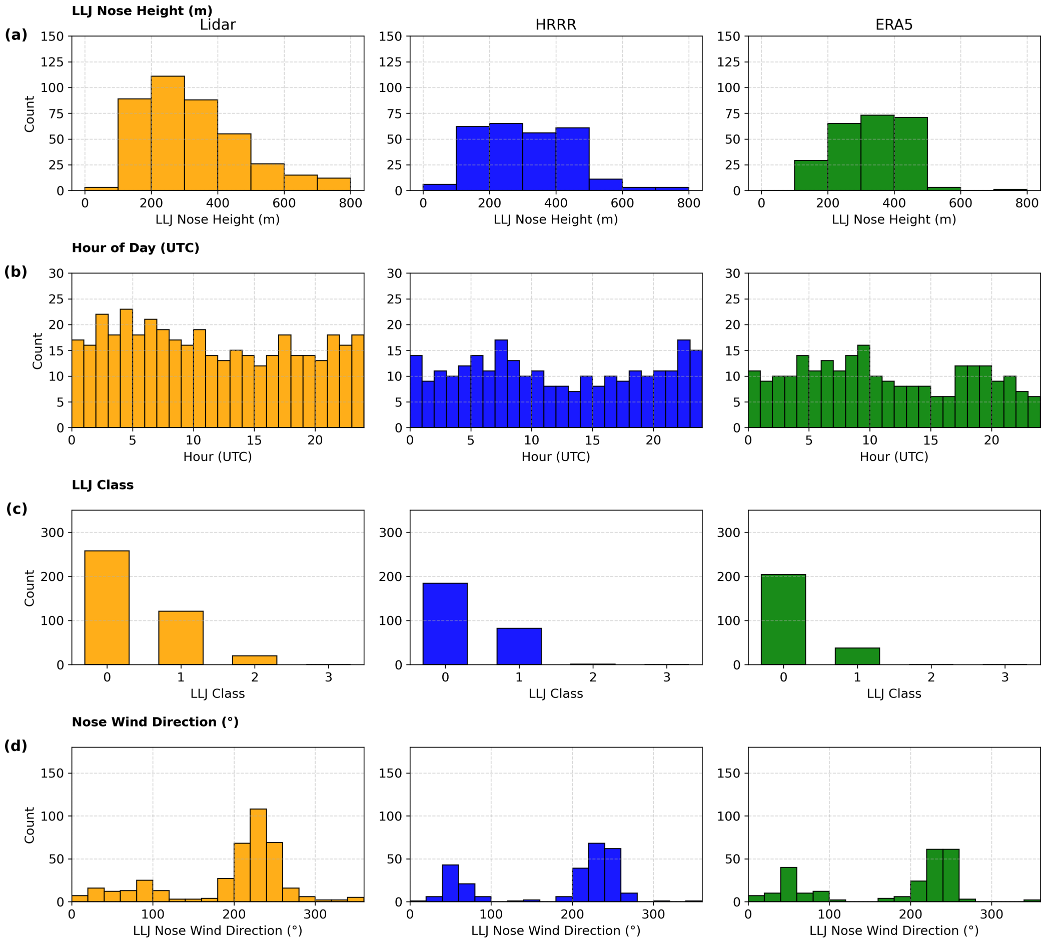

Figure 3. Histograms of LLJ characteristics from the lidar data (left), HRRR (center), and ERA5 (right). Four LLJ characteristics are shown: nose height (a), hour of the day when an LLJ is detected (b), LLJ class (c), and nose wind direction (d).

just above, and renewed warm biases aloft, with fewer statistically significant differences compared to the overall period.

4 Discussion and Conclusions

The WFIP3 observations provide new insights into the structure, frequency, and model representation of LLJs in the MABL of southern New England based on the first joint measurements of wind speed and temperature profiles from the WFIP3 barge. We show that LLJs occurred in more than 21% of observed profiles during summer 2024, with jet noses commonly near 300 m. LLJ occurrence shows only a weak diurnal preference for nighttime and early morning hours, consistent with synoptic-scale and baroclinic forcing being the dominant drivers rather than a classical nocturnal inertial oscillation mechanism. Both HRRR and ERA5 models captured general LLJ occurrence patterns and wind direction distributions but systematically underestimated wind speed and jet nose height under LLJ conditions. HRRR showed better performance than ERA5 in the lowest 250 m, but both models misrepresented the observed thermal structure. The thermal stratification errors are consistent with the regional SST biases documented by Adler et al. (2026), who showed that HRRR summer SSTs – which are forced by the Global Forecast System – are systematically warmer than observed along the U.S. Northeast Coast. Recent 3-way coupled modeling work from WFIP3 suggests that while high-resolution satellite SSTs or fully-coupled frameworks can ameliorate these near-surface differences, the resulting impacts are predominantly confined to the lowest 50 m of the marine boundary layer (Seo et al., 2025).

Compared to the modeling study of Aird et al. (2022), which reported peak LLJ frequencies of ∼12% in June with median jet heights around 150 m (using a different detection definition), our lidar data reveal a higher occurrence rate of over 21% and mean nose heights around 300 m. Our results also observationally benchmark the findings of Quint et al. (2025), who identified LLJs in 25% of hours from 1-year WRF simulations, with typical noses around 300 m and peak frequency during summer and nighttime hours.

Earlier observational studies are broadly consistent with our findings, though methodological differences require care in comparison. Helmis et al. (2013) documented summertime LLJs near Nantucket Island with nose heights of 150–300 m; their more permissive detection criterion (a 1.5 m s^{-1} decrease both above and below the nose) yields higher frequencies than our approach. Pichugina et al. (2017) detected LLJs in ∼63% of shipborne lidar profiles in the Gulf of Maine, with mean nose heights of ∼149 m; their higher frequency and lower noses likely reflect both a more permissive definition (no minimum nose speed threshold) and regional differences in baroclinic forcing. These comparisons underscore the sensitivity of LLJ statistics to detection methodology and sampling location, and motivate future cross-site analyses using consistent criteria. Our results also complement the continental LLJ analysis by Zhang et al. (2006), who reported frequent summertime nocturnal LLJs over the mid-Atlantic states, with jet altitudes averaging ∼670 m and peak occurrence during southwesterly flow. Our lower-altitude offshore LLJs are consistent in timing and wind direction but suggest enhanced frictional decoupling offshore.

We also highlight how the use of scanning lidars (or other instruments capable of profiling the entire MABL) is essential for a full characterization of offshore LLJs. Debnath et al. (2021) used buoy-mounted profiling lidars off the coast of New Jersey, with detection limited to 200 m above sea level. As our analysis shows, the majority of LLJ noses exceed this height, meaning that LLJs with noses above 200 m may be misclassified as monotonic high-shear events when only short-range measurements are available. Our results underscore the value—and rarity—of scanning lidar in offshore environments and highlight the need for expanded observational capabilities to fully characterize LLJs beyond the constraints of traditional profiling systems.

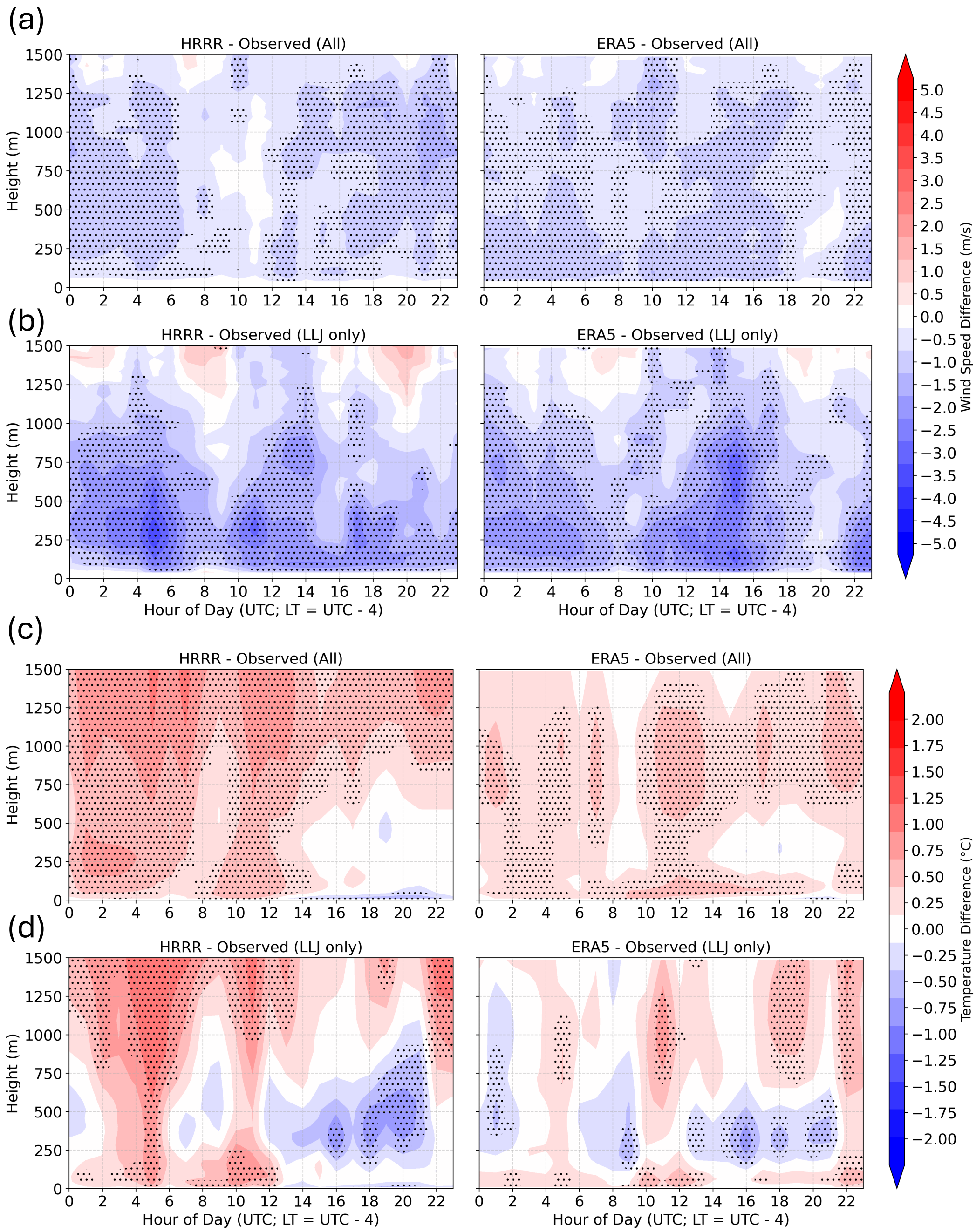

Figure 4. Average diurnal cycle of wind speed (a,b) and temperature (c,d) differences (model minus observation) at the offshore barge measurement site during summer 2024. Panels show differences for the HRRR (left column) and ERA5 (right column) models. (a) and (c) include all time periods (when observations are available) for wind speed and temperature, respectively, while (b) and (d) include only periods when an LLJ was detected in the observations. Differences are shown as a function of height and hour of the day (UTC). Mean wind speed and temperature differences were assessed for statistical significance using a bootstrap approach with 1000 resamples. Differences for which the 95% bootstrap confidence interval did not include 0 (i.e., statistically significant differences) are indicated with hatching.

Ultimately, this work supports efforts to refine offshore wind forecasting and reduce uncertainty in wind resource assessments: long-term, full-MABL profile offshore observations such as those from WFIP3 are essential for developing more physically realistic model representations of the MABL.

Open Research Section

Observations collected during the WFIP3 campaign are available at the Wind Data Hub (`https://wdh.energy.gov`). This study uses the two lidar datasets collected at the barge site (Bodini, 2025a, 2025b) and the thermodynamic profiles retrieved with TROPoe from the ASSIST instrument on the barge (Letizia, 2024). ERA5 data can be downloaded from the European Centre for Medium-Range Weather Forecasts (ECMWF, 2022). HRRR data are available at `www.nco.ncep.noaa.gov/pmb/products/hrrr/` and on the NOAA Open Data Dissemination at `registry.opendata.aws/noaa-hrrr-pds/`.

Conflict of Interest declaration

The authors declare there are no conflicts of interest for this manuscript.

Acknowledgments
This work was authored in part by the National Laboratory of the Rockies for the U.S. Department of Energy (DOE) under Contract No. DE-AC36-08GO28308. Funding provided by U.S. Department of Energy Office of Energy Efficiency and Renewable Energy Wind Energy Technologies Office and the NOAA Atmospheric Science for Renewable Energy Program. This research was supported by NOAA cooperative agreement NA22OAR4320151, for the Cooperative Institute for Earth System Research and Data Science (CIESRDS). Deployment of the Barge platform was supported by the Department of Energy award DE-EE0009424405 to the Woods Hole Oceanographic Institution and internal funds from the Woods Hole Oceanographic Institution. The views expressed in the article do not necessarily represent the views of the DOE, NOAA, or the U.S. Government. The U.S. Government retains and the publisher, by accepting the article for publication, acknowledges that the U.S. Government retains a nonexclusive, paid-up, irrevocable, worldwide license to publish or reproduce the published form of this work, or allow others to do so, for U.S. Government purposes.

References

Adler, B., Bianco, L., Turner, D. D., Olson, J. B., Sun, X., Gebauer, J., ... Wilczak, J. M. (2026). Multi-season evaluation of temperature and wind in the marine boundary layer along the United States northeast coast in the High-Resolution Rapid Refresh model. *EGUsphere [preprint]*. Retrieved from `https://doi.org/10.5194/egusphere-2026-97` doi: 10.5194/egusphere-2026-97

Aird, J. A., Barthelmie, R. J., Shepherd, T. J., & Pryor, S. C. (2022). Occurrence of low-level jets over the Eastern U.S. coastal zone at heights relevant to wind energy. *Energies*, *15*, 445. doi: 10.3390/en15020445

Angevine, W. M., Tjernström, M., & Žagar, M. (2006). Modeling of the coastal boundary layer and pollutant transport in New England. *J. Appl. Meteorol. Clim.*, *45*, 137–154. doi: 10.1175/JAM2333.1

Archer, C. L., Colle, B. A., Veron, D. L., Veron, F., & Sienkiewicz, M. J. (2016). On the predominance of unstable atmospheric conditions in the marine boundary layer offshore of the US northeastern coast. *J. Geophys. Res.-Atmos.*, *121*, 8869–8885. doi: 10.1002/2016JD024896

Baas, P., Bosveld, F. C., Baltink, H. K., & Holtslag, A. A. M. (2009). A climatology of nocturnal low-level jets at Cabauw. *J. Appl. Meteorol. Clim.*, *48*, 1627–

1642. doi: 10.1175/2009JAMC1965.1
Banta, R. M., Pichugina, Y. L., & Brewer, W. A. (2006). Turbulent velocity-variance profiles in the stable boundary layer generated by a nocturnal low-level jet. *Journal of the Atmospheric Sciences*, *63*, 2700–2719.
Barthelmie, R. J., Dantuono, K. E., Renner, E. J., Letson, F. L., & Pryor, S. C. (2021). Extreme wind and waves in US East Coast offshore wind energy lease areas. *Energies*, *14*, 1053. doi: 10.3390/en14041053
Blackadar, A. K. (1957). Boundary layer wind maxima and their significance for the growth of nocturnal inversions. *B. Am. Meteorol. Soc.*, *38*, 283–290. doi: 10.1175/1520-0477-38.5.283
Bodini, N. (2025a). *WFIP3 – BARG site – NREL Lidar (z01) [Dataset].* Wind Data Hub, maintained for the U.S. Department of Energy, Office of Energy Efficiency and Renewable Energy. Retrieved from `https://doi.org/10.21947/2345993` (Accessed: 2026-06-17) doi: 10.21947/2345993
Bodini, N. (2025b). *WFIP3 – BARG site – NREL Lidar (z02) [Dataset].* Wind Data Hub, maintained for the U.S. Department of Energy, Office of Energy Efficiency and Renewable Energy. Retrieved from `https://doi.org/10.21947/2569228` (Accessed: 2026-06-17) doi: 10.21947/2569228
Bodini, N., Lundquist, J. K., & Kirincich, A. (2019, May). U.S. East Coast lidar measurements show offshore wind turbines will encounter very low atmospheric turbulence. *Geophysical Research Letters*, *46*(10), 5582–5591. Retrieved from `https://doi.org/10.1029/2019GL082636` (Open Access) doi: 10.1029/2019GL082636
Bosart, L. F., & Sanders, F. (1981). The Johnstown flood of July 1977: A long-lived convective system. *Journal of the Atmospheric Sciences*, *38*, 1616–1642.
Christiansen, M. B., & Hasager, C. B. (2005). Wake effects of large offshore wind farms identified from satellite SAR. *Remote Sens. Environ.*, *98*, 251–268.
Debnath, M., Doubrawa, P., Optis, M., Hawbecker, P., & Bodini, N. (2021). Extreme wind shear events in US offshore wind energy areas and the role of induced stratification. *Wind Energ. Sci.*, *6*, 1043–1059. doi: 10.5194/wes-6-1043-2021
de Jong, E., Quon, E., & Yellapantula, S. (2023). Mechanisms of low-level jet formation in the U.S. Mid-Atlantic offshore. *J. Atmos. Sci.*, *81*, 31–52. doi: 10.1175/JAS-D-23-0079.1
Dowell, D. C., Alexander, C. R., James, E. P., Weygandt, S. S., Benjamin, S. G., Manikin, G. S., … Alcott, T. I. (2022). The High-Resolution Rapid Refresh (HRRR): An hourly updating convection-allowing forecast model. Part i: Motivation and system description. *Weather and Forecasting*, *37*(8), 1371–1395. doi: 10.1175/WAF-D-21-0151.1
European Centre for Medium-Range Weather Forecasts. (2022). *ERA5 reanalysis model level data [dataset].* NSF National Center for Atmospheric Research. Retrieved from `https://doi.org/10.5065/XV5R-5344` (Accessed 13 Oct 2025) doi: 10.5065/XV5R-5344
Floors, R., Vincent, C. L., Gryning, S. E., et al. (2013). The Wind Profile in the Coastal Boundary Layer: Wind Lidar Measurements and Numerical Modelling. *Boundary-Layer Meteorology*, *147*, 469–491. doi: 10.1007/s10546-012-9791-9
Gottschall, J., Wolken-Möhlmann, G., Viergutz, T., & Lange, B. (2014). Results and conclusions of a floating-lidar offshore test. *Energy Proc.*, *53*, 156–161. doi: 10.1016/j.egypro.2014.07.224
Gutierrez, W., Ruiz-Columbie, A., Tutkun, M., & Castillo, L. (2017). Impacts of the low-level jet's negative wind shear on the wind turbine. *Wind Energy Science*, *2*, 533–545. Retrieved from `https://doi.org/10.5194/wes-2-533-2017` doi: 10.5194/wes-2-533-2017
Hallgren, C., Aird, J. A., Ivanell, S., Körnich, H., Barthelmie, R. J., Pryor, S. C., & Sahlée, E. (2023). Brief communication: On the definition of

the low-level jet. *Wind Energy Science*, *8*, 1651–1658. Retrieved from https://doi.org/10.5194/wes-8-1651-2023 doi: 10.5194/wes-8-1651-2023

Hallgren, C., Arnqvist, J., Ivanell, S., Körnich, H., Vakkari, V., & Sahlée, E. (2020). Looking for an Offshore Low-Level Jet Champion among Recent Reanalyses: A Tight Race over the Baltic Sea. *Energies*, *13*, 3670. doi: 10.3390/en13143670

Helmis, C. G., Wang, Q., Sgouros, G., Wang, S., & Halios, C. (2013). Investigating the summertime low-level jet over the East Coast of the U.S.A.: A case study. *Boundary-Layer Meteorology*, *149*(2), 259–276. Retrieved from https://doi.org/10.1007/s10546-013-9841-y (Published online: 24 July 2013) doi: 10.1007/s10546-013-9841-y

Hersbach, H., Bell, B., Berrisford, P., Hirahara, S., Horányi, A., Muñoz-Sabater, J., ... Thépaut, J.-N. (2020). The ERA5 global reanalysis. *Quarterly Journal of the Royal Meteorological Society*, *146*(730), 1999–2049. doi: 10.1002/qj.3803

Holton, J. R. (1967). The diurnal boundary layer wind oscillation above sloping terrain. *Tellus*, *19*, 199–205. doi: 10.1111/j.2153-3490.1967.tb01473.x

James, E. P., Alexander, C. R., Dowell, D. C., Weygandt, S. S., Benjamin, S. G., Manikin, G. S., ... Turner, D. D. (2022). The High-Resolution Rapid Refresh (HRRR): an hourly updating convection-allowing forecast model. Part ii: Forecast performance. *Weather and Forecasting*, *37*(8), 1397–1417. doi: 10.1175/WAF-D-21-0130.1

Kalverla, P. C., Holtslag, A. A. M., Ronda, R. J., & Steeneveld, G. J. (2020). Quality of wind characteristics in recent wind atlases over the North Sea. *Quarterly Journal of the Royal Meteorological Society*, *146*, 1498–1515. doi: 10.1002/qj.3748

Krishnamurthy, R., García Medina, G., Gaudet, B., Gustafson, W. I., Jr., Kassianov, E. I., Liu, J., ... Mahon, A. M. (2023). Year-long buoy-based observations of the air–sea transition zone off the US west coast. *Earth System Science Data*, *15*, 5667–5699. Retrieved from https://doi.org/10.5194/essd-15-5667-2023 doi: 10.5194/essd-15-5667-2023

Letizia, S. (2024). *WFIP3 – NREL ASSIST Barge / Thermodynamic Retrievals TROPoe [Dataset].* Wind Data Hub, maintained for the U.S. Department of Energy, Office of Energy Efficiency and Renewable Energy. Retrieved from https://doi.org/10.21947/2473243 (Accessed: 2026-06-17) doi: 10.21947/2473243

Letizia, S., Michaud-Belleau, V., Turner, D. D., & Abraham, A. (2025). *Thermodynamic Profiling Through ASSIST Observations and TROPoe Retrievals* (Tech. Rep. No. NREL/TP-5000-92509). Golden, CO: National Renewable Energy Laboratory. Retrieved from https://www.nrel.gov/docs/fy26osti/92509.pdf

Liu, H., He, M., Wang, B., et al. (2014). Advances in low-level jet research and future prospects. *Acta Meteorologica Sinica*, *28*, 57–75. doi: 10.1007/s13351-014-3166-8

Lundquist, J. K., DuVivier, K. K., Kaffine, D., & Tomaszewski, J. M. (2019). Costs and consequences of wind turbine wake effects arising from uncoordinated wind energy development. *Nature Energy*, *4*, 26–34. doi: 10.1038/s41560-018-0281-2

Mahrt, L., Vickers, D., & Andreas, E. L. (2014). Low-level wind maxima and structure of the stably stratified boundary layer in the coastal zone. *J. Appl. Meteorol. Clim.*, *53*, 363–376. doi: 10.1175/JAMC-D-13-0170.1

Michaud-Belleau, V., Gaudreau, M., Lacoursière, J., Boisvert, É., Ravelomanantsoa, L., Turner, D. D., & Rochette, L. (2025). The Atmospheric Sounder Spectrometer by Infrared Spectral Technology (ASSIST): Instrument design and signal processing. *EGUsphere [preprint]*. Retrieved from https://doi.org/10.5194/egusphere-2024-3617 doi: 10.5194/egusphere-2024-3617

Myers, T. A., Van Ormer, A., Turner, D. D., Wilczak, J. M., Bianco, L., & Adler, B.

(2024, October). Evaluation of hub-height wind forecasts over the New York Bight. *Wind Energy*, *27*(10), 1063–1073. doi: 10.1002/we.2936

Newsom, R. K., Brewer, W. A., Wilczak, J. M., Wolfe, D. E., Oncley, S. P., & Lundquist, J. K. (2017). Validating precision estimates in horizontal wind measurements from a doppler lidar. *Atmospheric Measurement Techniques*, *10*, 1229–1240. Retrieved from `https://doi.org/10.5194/amt-10-1229-2017` doi: 10.5194/amt-10-1229-2017

Newsom, R. K., Gibler, G., Gaustad, K., & Zhang, D. (2024). *Doppler Lidar Motion-Correction (DLMC) Value-Added Product Report* (Tech. Rep. No. DOE/SC-ARM-TR-296). Richland, Washington: U.S. Department of Energy, Atmospheric Radiation Measurement user facility. Retrieved from `https://doi.org/10.2172/2318487` doi: 10.2172/2318487

Newsom, R. K., Sivaraman, C., Shippert, T. R., & Riihimaki, L. D. (2019). *Doppler Lidar Vertical Velocity Statistics Value-Added Product* (Tech. Rep. No. April). Department of Energy ARM. Retrieved from `https://www.osti.gov/servlets/purl/1238068`

Olson, J. B., Kenyon, J. S., Djalalova, I., Bianco, L., Turner, D. D., Pichugina, Y., … Cline, J. (2019). Improving wind energy forecasting through numerical weather prediction model development. *Bulletin of the American Meteorological Society*, *100*(11), 2201–2220. doi: 10.1175/BAMS-D-18-0040.1

Patton, E. G., Sullivan, P. P., Kosović, B., Dudhia, J., Mahrt, L., Žagar, M., & Marić, T. (2019). On the influence of swell propagation angle on surface drag. *J. Appl. Meteorol. Climatol.*, *58*, 1039–1059. doi: 10.1175/JAMC-D-18-0211.1

Pearson, G., Davies, F., & Collier, C. (2009, February). An analysis of the performance of the UFAM pulsed doppler lidar for observing the boundary layer. *Journal of Atmospheric and Oceanic Technology*, *26*(2), 240–250. doi: 10.1175/2008JTECHA1128.1

Pichugina, Y. L., Brewer, W. A., Banta, R. M., Choukulkar, A., Clack, C. T. M., Marquis, M. C., … Hardesty, R. M. (2017). Properties of the offshore low level jet and rotor layer wind shear as measured by scanning Doppler lidar: Offshore low level jet from scanning doppler lidar measurements. *Wind Energy*, *20*, 987–1002. doi: 10.1002/we.2075

Platis, A., Siedersleben, S. K., Bange, J., Lampert, A., Bärfuss, K., Hankers, R., … Emeis, S. (2018). First in situ evidence of wakes in the far field behind offshore wind farms. *Sci. Rep.*, *8*, 2163. doi: 10.1038/s41598-018-20389-y

Pronk, V., Bodini, N., Optis, M., Lundquist, J. K., Moriarty, P., Draxl, C., … Young, E. (2022). Can reanalysis products outperform mesoscale numerical weather prediction models in modeling the wind resource in simple terrain? *Wind Energ. Sci.*, *7*, 487–504. doi: 10.5194/wes-7-487-2022

Quint, D., Lundquist, J. K., & Rosencrans, D. (2025). Simulations suggest offshore wind farms modify low-level jets. *Wind Energy Science*, *10*(1), 117–142.

Rife, D. L., Pinto, J. O., Monaghan, A. J., Davis, C. A., & Hannan, J. R. (2010). Global distribution and characteristics of diurnally varying low-level jets. *J. Climate*, *23*, 5041–5064. doi: 10.1175/2010JCLI3514.1

Rubio, H., Kühn, M., & Gottschall, J. (2022). Evaluation of low-level jets in the southern Baltic Sea: a comparison between ship-based lidar observational data and numerical models. *Wind Energy Science*, *7*, 2433–2455. Retrieved from `https://doi.org/10.5194/wes-7-2433-2022` doi: 10.5194/wes-7-2433-2022

Schulz-Stellenfleth, J., Emeis, S., Dörenkämper, M., Bange, J., Cañadillas, B., Neumann, T., … Lampert, A. (2022). Coastal impacts on offshore wind farms – a review focussing on the German Bight area. *Meteorologische Zeitschrift*, *31*, 289–315. doi: 10.1127/metz/2022/1109

Seo, H., Sauvage, C., Renkl, C., Lundquist, J. K., & Kirincich, A. (2025, November). Sea surface warming and ocean-to-atmosphere feedback driven by large-scale offshore wind farms under seasonally stratified conditions. *Science Advances*, *11* (45), eadw7603. doi: 10.1126/sciadv.adw7603

Shaw, W. J., Berg, L. K., Debnath, M., Deskos, G., Draxl, C., Ghate, V. P., ... Wilczak, J. M. (2022). Scientific challenges to characterizing the wind resource in the marine atmospheric boundary layer. *Wind Energy Science*, *7*, 2307–2334. Retrieved from `https://doi.org/10.5194/wes-7-2307-2022` doi: 10.5194/wes-7-2307-2022

Shaw, W. J., Draher, J., Garcia Medina, G., Gorton, A. M., Krishnamurthy, R., Newsom, R. K., ... Yang, Z. (2020). *General analysis of data collected from DOE lidar buoy deployments off Virginia and New Jersey* (Tech. Rep. No. PNNL-29823). Pacific Northwest National Laboratory. doi: 10.2172/1632348

Storm, B., Dudhia, J., Basu, S., Swift, A., & Giammanco, I. (2008). Evaluation of the Weather Research and Forecasting Model on forecasting low-level jets: Implications for wind energy. *Wind Energy*, *12*, 81–90. doi: 10.1002/we.288

Su, J., Felton, M., Lei, L., McCormick, M. P., Delgado, R., & St. Pé, A. (2016). Lidar remote sensing of cloud formation caused by low-level jets. *Journal of Geophysical Research: Atmospheres*, *121* (10), 5904–5911. doi: 10.1002/2015JD024590

Turner, D. D., & Blumberg, W. G. (2019). Improvements to the AERIoe thermodynamic profile retrieval algorithm. *IEEE Journal of Selected Topics in Applied Earth Observations and Remote Sensing*, *12*, 1339–1354. doi: 10.1109/JSTARS.2018.2874968

Turner, D. D., & Löhnert, U. (2014). Information content and uncertainties in thermodynamic profiles and liquid cloud properties retrieved from the ground-based Atmospheric Emitted Radiance Interferometer (AERI). *Journal of Applied Meteorology and Climatology*, *53* (3), 752–771. doi: 10.1175/JAMC-D-13-0126.1

Turner, D. D., & Löhnert, U. (2021). Ground-based temperature and humidity profiling: combining active and passive remote sensors. *Atmospheric Measurement Techniques*, *14*, 3033–3048. doi: 10.5194/amt-14-3033-2021

Vanderwende, B. J., Lundquist, J. K., Rhodes, M. E., Takle, E. S., & Irvin, S. L. (2015). Observing and simulating the summertime low-level jet in central Iowa. *Monthly Weather Review*, *143* (6), 2319–2336.

Veers, P., Dykes, K., Lantz, E., Barth, S., Bottasso, C. L., Carlson, O., ... Wiser, R. (2019). Grand challenges in the science of wind energy. *Science*, *366*, eaau2027. doi: 10.1126/science.aau2027

Viselli, A., Filippelli, M., Pettigrew, N., Dagher, H., & Faessler, N. (2019). Validation of the first lidar wind resource assessment buoy system offshore the Northeast United States. *Wind Energy*, *22*, 1548–1562. doi: 10.1002/we.2387

Wagner, D., Steinfeld, G., Witha, B., Wurps, H., & Reuder, J. (2019). Low Level Jets over the Southern North Sea. *Meteorologische Zeitschrift*, *28* (5), 389–415.

Zhang, D.-L., Zhang, S., & Weaver, S. (2006). Low-level jets over the Mid-Atlantic States: Warm-season climatology and a case study. *Journal of Applied Meteorology and Climatology*, *45* (1), 194–209. doi: 10.1175/JAM2313.1